

# Disintegration Mechanism of Coal-Bearing Soil Based on Granularity Entropy and Water–Air Two-Phase Flow

Guanji Lyu, Mingxin Zheng,\* Lu Xiong, Zilong Liu, and Hanqiu Zhang



Cite This: *ACS Omega* 2025, 10, 1667–1676



Read Online

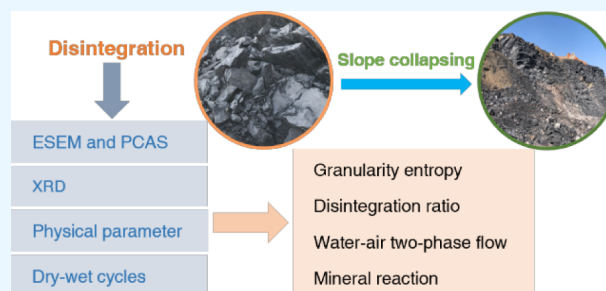
ACCESS |

Metrics & More

Article Recommendations

**ABSTRACT:** Coal-bearing soils (CBS), products of coal-bearing strata weathering, are particularly prone to disintegration due to the effects of dry-wet cycles. Static water disintegration tests, environmental scanning electron microscopy (ESEM), and mineral chemical composition analyses were conducted on CBS. The disintegration evolution of CBS is characterized by granularity entropy and is analyzed concerning the disintegration ratio. Furthermore, the disintegration mechanism is examined based on the water–air two-phase flow (WTF) and mineral chemical reactions. Results show a significant exponential relationship between the standard basic entropy ( $A$ ) and disintegration ratio ( $D_R$ ), where the disintegration

ratio decreases as the standard basic entropy increases. As the number of dry-wet cycles increases,  $A$  initially decreases rapidly before stabilizing, mirroring the variation pattern of the particle size distribution curve and its derived indicators. Illite produces significant short-range hydration repulsion, leading to the formation of additional cracks in CBS. WTF significantly influences disintegration; water intrusion increases air pressure, and the subsequent pressure release plays a critical role in damaging soil structure. These findings are significant for the safety and protection of CBS slope engineering.



## 1. INTRODUCTION

Coal-bearing soils (CBS) refer to the exposed weathered soft rocks of coal systems, characterized by a loose structure and the presence of fissures. CBS are widely distributed in the hilly areas of Jiangxi, Guangdong, Guangxi, Sichuan, and other provinces in China, and they are commonly encountered in civil engineering.<sup>1</sup> The macroscopic disintegration of CBS, when saturated with water, manifests as exfoliation and dispersion into flaky or granular masses, while microscopically, it involves structural damage, deterioration, and transformation into mud. In particular, the physical and mechanical properties of CBS have been significantly altered by rainstorm climates and dry-wet cycles in southern China.<sup>2,3</sup> Such structural degradation leads to a marked reduction in strength indicators, often resulting in slumping or landslides on slopes within road and railway construction areas. For example, several CBS slopes collapsed during the construction of the K201–K213 section of the Changli Expressway in Jiangxi Province. Furthermore, CBS disintegration can result in uneven foundation settlement, affecting the safety of high-speed trains.<sup>4,5</sup> In conclusion, the disintegration of CBS compromises the integrity of the soil structure and can lead to serious disasters such as landslides and uneven settlement, underscoring the importance of studying the disintegration characteristics of CBS.

Significant research has been conducted by scholars on the quantitative characterization of particles following the dis-

integration of soft rocks. Zhang et al.<sup>6</sup> proposed an equation to calculate the disintegration index based on an evolutionary model. Chen et al.<sup>7</sup> analyzed the fractal characteristics of red bedded chondrites under load, while Zhang et al.<sup>8</sup> utilized disintegration ratios for characterization. Ding et al.<sup>9</sup> developed a model for changes in the fractal dimension of slate disintegration over time. However, a standardized approach for quantifying particle disintegration in soft rocks, including CBS, is lacking. Given the complexity of the CBS disintegration mechanism, investigating granularity entropy for its quantitative characterization is warranted.

The disintegration of CBS under dry-wet cycles has garnered significant attention. Many scholars contend that the disintegration of soft rocks is primarily attributed to water absorption, which is closely associated with the composition and content of clay minerals.<sup>6,10–13</sup> The disintegration of soft rocks is influenced by physical, chemical, and anthropogenic factors.<sup>2,14,15</sup> CBS exhibits unique disintegration characteristics compared to other soft rocks, heavily influenced by water

**Received:** October 21, 2024  
**Revised:** December 11, 2024  
**Accepted:** December 17, 2024  
**Published:** December 26, 2024



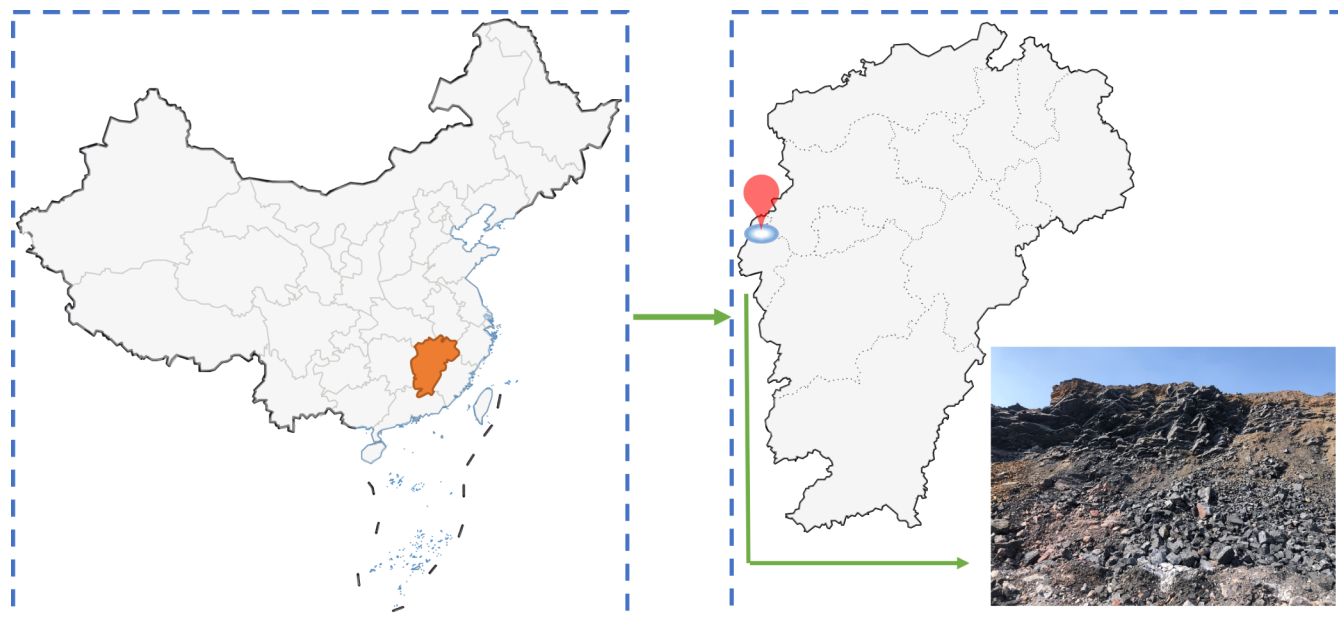


Figure 1. Location of sampling.

content. Scholars have observed that the shear strength of CBS decreases with increased water content, notably affecting cohesion more than the angle of internal friction.<sup>16,17</sup> Dry-wet cycles induce significant changes not only in the mechanical properties but also in the microstructure of CBS. Zhang et al.<sup>18</sup> employed discrete elements for numerical modeling to assess fine-scale parameters, while Fan et al.<sup>16</sup> correlated these mechanical properties with microstructural changes. Huang et al.<sup>19</sup> explored the residual strength and microstructural attributes of CBS under dry-wet cycles, and Gu et al.<sup>20</sup> investigated crack expansion and dynamic properties. Naturally, CBS contains water and air phases, making it vulnerable to transient infiltration during initial immersion, where trapped air raises pressure, severely impacting soil structure. Caron et al.<sup>21,22</sup> studied air pressure dynamics and material stability during immersion, while Grant et al.<sup>23</sup> highlighted the disruptive effect of transient pore air pressure on soil microstructure. The research on CBS is still in its early stages, and the disintegration theory remains imperfect. Specifically, there have been no reports on the impact of WTF on the disintegration of CBS.

We utilized granularity entropy theory to quantitatively describe the changes in particle content during CBS disintegration and to investigate the disintegration characteristics of CBS under dry-wet cycles. We established a correlation between the granularity entropy parameter and the disintegration ratio, and derived the relationship between the granularity entropy parameter and the number of dry-wet cycles. Based on the mineral composition and pore structure characteristics of CBS, we analyzed WTF and the physicochemical reactions of minerals to reveal the mechanism of CBS disintegration. This study quantitatively characterizes the disintegration of CBS from a new perspective. Additionally, WTF was integrated with macroscopic and microscopic methods to analyze the disintegration mechanism, providing a fundamental interpretation of CBS disintegration and mudification, thus deepening the theory of unsaturated CBS. This research offers a theoretical basis and technical support for risk control and landslide disaster management of CBS

slopes, and it also serves as a reference for studying other adverse soil collapse characteristics.

## 2. SAMPLES AND TEST METHODS

**2.1. Basic Properties of the Sample.** The CBS samples were collected from K207 + 613 on the Changli Expressway, as illustrated in Figure 1. CBS is primarily a result of intense (complete) weathering of the parent rock, predominantly in the form of gravel, and appears dark gray to black with a glassy luster on the surface. Our research group utilized the D8 ADVANCE X-ray diffractometer manufactured by the German company Bruker to identify the mineral composition of CBS. The proportion of the mineral composition of CBS determined by the experiment is presented in Figure 2. Additionally, the

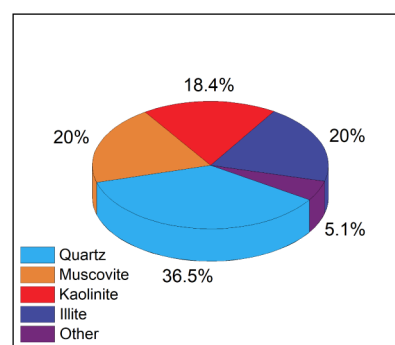


Figure 2. Proportion of mineral composition in CBS.

chemical composition of CBS was analyzed using a comprehensive chemical analysis method, as shown in Figure 3. The fundamental physical and mechanical properties are summarized in Table 1, where the compression modulus and compression coefficient were tested at a compaction degree of 93%.

The mineral composition of soil primarily consists of primary minerals and secondary minerals. Primary minerals are the products of physical weathering of the parent rock, exhibiting no significant changes in chemical composition, only

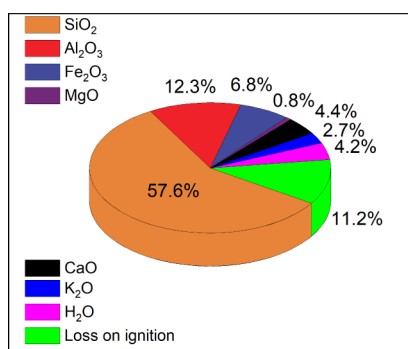


Figure 3. Proportion of chemical composition in CBS.

Table 1. Basic Physical Properties of CBS

Parameter	Value
$w_0$	2.24%
$w_{sat}$	14.14%
$w_p$	19.3
$w_L$	27.4
$I_p$	8.1
$w_{OP}$	10.4
$\rho_{dmax}$	1.835 g/cm <sup>3</sup>
$\alpha_{1-2}$	0.0827 MPa <sup>-1</sup>
$E_s$	18.25 MPa

alterations in shape and particle size. Representative primary minerals include quartz, feldspar, and mica. In contrast, secondary minerals are newly formed minerals that arise during the weathering process as the parent rock transforms into soil. These minerals are generated through further chemical reactions, such as oxidation, hydration, hydrolysis, and dissolution of primary minerals. Secondary minerals are mainly composed of hydrated aluminosilicates formed by the decomposition of silicate minerals, specifically clay minerals, with representative examples including Illite and kaolinite. Consequently, soil samples typically exhibit characteristics such as low compressibility, poor hydrophilicity, slight swelling and shrinkage, and low plasticity.<sup>24</sup>

**2.2. Test Methods. 2.2.1. ESEM and PCAS.** The ESEM (Environmental Scanning Electron Microscopy) experiment was conducted using the Quanta250 scanning electron microscope manufactured by FEI (USA), as shown in Figure 4. The electron beam source in this microscope is a tungsten filament. PCAS is a specialized software designed for the identification and quantitative analysis of pore and crack systems. It has been successfully applied to the quantitative identification and structural analysis of pores and cracks in rock and soil.<sup>25,26</sup>

**2.2.2. Static Water Disintegration Test.** The static water disintegration test primarily involves immersing the selected natural state soil sample in water, carefully observing its disintegration process, and assessing its disintegration rate and degree. Upon completion of the disintegration, the disintegrated material is dried for particle analysis, and changes in its gradation are examined. The experimental program design is illustrated in Figure 5. We conducted 25 dry-wet cycle tests to comprehensively study the disintegration and evolution of soft rocks in CBS. The samples consist of approximately equal-sized, nonsharp corner specimens to minimize the interference of initial shape differences on the test results. The soaking time for the samples in each dry-wet cycle is set to 12 h.<sup>8</sup> Each



Figure 4. ESEM testing machine.

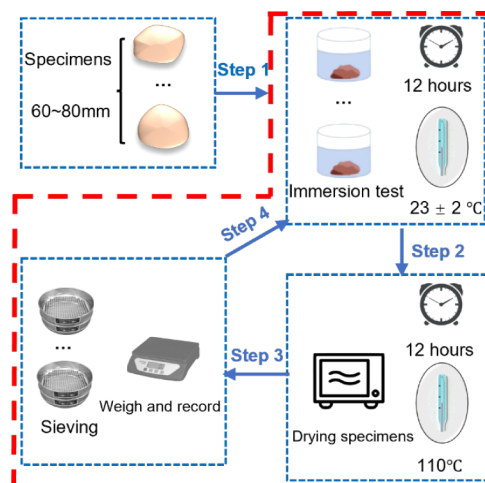


Figure 5. Experimental procedure for dry-wet cycles of CBS.

sample is dried in a 110 °C oven for 12 h before each test (except for the initial immersion). Standard sieves with pore sizes of 60, 40, 20, 10, 5, 2, 1, 0.5, 0.25, and 0.075 mm are used for sieve analysis of the disintegrated products. Additionally, efforts are made to maintain the natural state of fragmentation and disintegration to minimize the influence of external conditions on the degree of sample disintegration. The screening test omits the use of a vibrating screen machine and employs a manual layer-by-layer vibration method instead. In Figure 5, the red dashed line represents the procedure for the repeated dry-wet cycle tests.

### 3. RESULTS

**3.1. Pore Morphology Characteristics.** We utilized PCAS software to analyze the ESEM images of CBS, with a sample magnification of 1000x. Figure 6 presents the ESEM image alongside the PCAS-processed image of CBS.



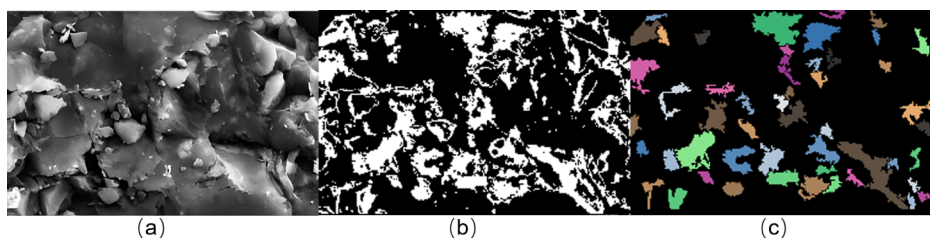


**Figure 6.** Original ESEM image and PCAS-processed image: (a) the original ESEM image, (b) the binary image generated by PCAS, (c) Pores distinguished by color.

Specifically, Figure 6a displays the original ESEM image of CBS, while Figure 6b illustrates the binary image generated by the PCAS software. Figure 6c presents the imaging results, where different colors are employed to distinguish between various pores.

The pore-related parameters obtained from the PCAS analysis are presented in Table 2. The porosity ratio of CBS

**Table 2.** Pore-related Parameters Obtained from PCAS Analysis

Parameter	Value
Total region area	8899 $\mu\text{m}^2$
Porosity	18.34%
Average region area	171.13 $\mu\text{m}^2$
Average length	23 $\mu\text{m}$
Average form factor	0.3722
Average width	13.52 $\mu\text{m}$
Probability entropy	0.9141
Fractal dimension	1.2072

is 18.34%. The shape factor, which reflects the roughness of the pore edges, has a maximum value of 1. A smaller shape factor indicates a rougher pore edge and a more complex corresponding structure; the shape factor for CBS is 0.3722. Probability entropy quantifies the orientation of pores, with the measured probability entropy of CBS being 0.9141. A larger value indicates a more nondirectional development of the pores. The fractal dimension describes the degree of variation of parameters within a certain range, representing the heterogeneity of the data. The fractal dimension of CBS is 1.2072.

**3.2. Static Water Disintegration Test Results.** Figure 7 illustrates the changes in particle size content of CBS across

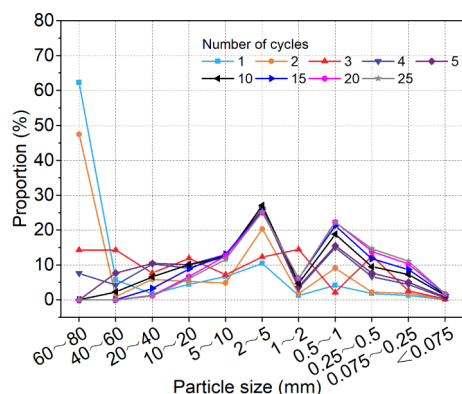


**Figure 7.** Proportion of particle sizes in CBS across different dry-wet cycles.

different dry-wet cycles, while Figure 8 presents the particle size distribution curve for CBS under the same conditions.

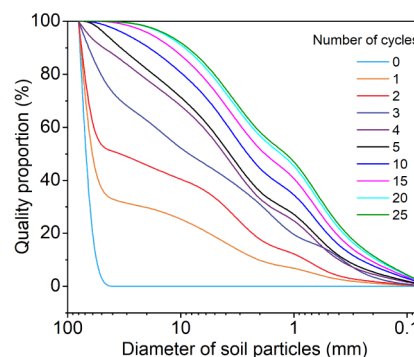


**Figure 8.** Particle size distribution curves of CBS across different dry-wet cycles.

During the initial 0 to 25 cycles, the particle size of the samples undergoes significant changes. The content of particles with a diameter greater than 60 mm rapidly decreases from 100% to 0%. Concurrently, the content of coarse particles within the size range of 5 to 60 mm declines as the number of cycles increases. In contrast, there is no significant change in the particle content within the size range of 1 to 5 mm. However, the particle content in the size range of 0.075 to 1 mm increases substantially with the number of cycles. This indicates that particles in the size range of 5 to 60 mm are being transformed into those in the range of 0.075 to 1 mm, while the content of fine particles continues to rise slowly, remaining within 2%. These observations suggest that the disintegration of CBS samples primarily occurs in the coarse particle size range of 5 to 60 mm during cycles 5 to 25. As the number of dry-wet cycles increases, the particle size distribution curve continuously evolves, and its shape becomes more similar, as seen in the curves for 20 and 25 dry-wet cycles.

## 4. DISCUSSION

**4.1. Granularity Entropy.** Entropy was originally utilized to describe the probability and disorder of states within thermodynamic systems. Subsequently, the concept of statistical entropy was introduced to quantify the uncertainty associated with system information.<sup>27,28</sup> In a discrete system comprising  $m$  identical boxes, let the  $i$ -th box contain  $M_i$  units. The entire system contains  $M$  units, and the statistical entropy of the system is represented by the formula (1). Here,  $s$  denotes the unit entropy, and  $\alpha_i$  represents the frequency of the  $i$ -th box. When there are only two boxes, the maximum entropy value of the system is 1, which occurs when  $\alpha_1 = \alpha_2 = 0.5$ .

$$\begin{cases} S_S = MS \\ S = -\frac{1}{\ln 2} \sum_{i=1}^M \alpha_i \ln \alpha_i \\ \alpha_i = \frac{M_i}{M} \end{cases} \quad (1)$$

According to the definition of statistical entropy, the width of each box is uniform. To apply the concept of statistical entropy, the  $[\text{SiO}_4]^{4-}$  tetrahedral height of  $-2^{22}$  mm is selected as the unit box width.<sup>29</sup> Lrincz defined the concept of “truncation” by embedding unit boxes into a truncation.<sup>30</sup> Considering the wide range of particle sizes in geotechnical media, the truncation size generally increases proportionally by multiples of 2. However, the commonly used standard sieve apertures do not increase in a proportional manner. The cutoff sizes are set according to the standard sieve apertures, and the range of the  $i$ -th truncated particle size  $d_i$  is obtained as shown in formula (2). By substituting formula (3) into formula (1) and further processing, formulas (4–6) can be derived. Any particle size distribution curve can be quantified based on the mapping relationship ( $f_1: \Delta \rightarrow [S_0, \Delta S]$  or  $f_n: \Delta \rightarrow [A, B]$ ) between the above distribution curve and two granularity entropy parameters.<sup>31,32</sup>

$$\begin{cases} D_i \geq d \geq D_{i-1} (i = 1, 2, \dots, n) \\ C_i = \frac{D_i - D_{i-1}}{d_0} = 2^{22} \Delta D_i \end{cases} \quad (2)$$

$$\begin{cases} \alpha_j = \frac{P_j}{C_i} (j = 1, 2, \dots, C_i) \\ \sum_{i=1}^N P_i = 1 \end{cases} \quad (3)$$

$$\begin{aligned} S &= S_0 + \Delta S \\ &= -\frac{1}{\ln 2} \sum_{i=1}^N C_i \frac{P_i}{C_i} \ln \left( \frac{P_i}{C_i} \right) \\ &= \sum_{i=1}^N P_i \frac{\ln C_i}{\ln 2} + \left( -\frac{1}{\ln 2} \sum_{i=1}^N P_i \ln P_i \right) \end{aligned} \quad (4)$$

$$\begin{aligned} A &= \frac{S_0 - S_{0\min}}{S_{0\max} - S_{0\min}} \\ &= \frac{\sum_{i=1}^N P_i \frac{\ln C_i}{\ln 2} - \frac{\ln C_1}{\ln 2}}{\frac{\ln C_N}{\ln 2} - \frac{\ln C_1}{\ln 2}} \\ &= \frac{\sum_{i=1}^N P_i \ln \left( \frac{\Delta D_i}{\Delta D_1} \right)}{\ln \left( \frac{\Delta D_n}{\Delta D_1} \right)} \end{aligned} \quad (5)$$

$$B = \frac{\Delta S}{\ln N} = \frac{-\frac{1}{\ln 2} \sum_{i=1}^N P_i \ln P_i}{\ln N} \quad (6)$$

Where  $N$  is the number of truncations included between the maximum and minimum particle sizes.  $D_i$  ( $i = 0, 1, 2, \dots, N$ ) is a truncated size sequence.  $C_i$  is the number of unit boxes within

the  $i$ -th truncation.  $d_0$  is the width of each unit box.  $\Delta D_i$  is the width of the  $i$ -th truncation.  $P_i$  is the  $i$ -th truncated particle content. Assuming that the particles are uniformly distributed within the truncation,  $\alpha_i$  is the probability of the  $i$ -th truncated particle being within the basic unit  $j$ .

#### 4.2. Characterization of Granularity Entropy of CBS.

Currently, researchers have incorporated the granularity entropy analysis method into the study of particle size distribution to describe the disintegration and fragmentation of rocks, demonstrating both accuracy and effectiveness.<sup>32,33</sup> Following the concept of the disintegration ratio proposed by Erguler et al.,<sup>34</sup> the area enclosed by the vertical lines at 0.075 mm and 80 mm above each particle size distribution curve is calculated. The disintegration ratio ( $D_R$ ) is defined as the ratio of the area difference ( $A_1$ ) between the dry-wet cycle and the initial state to the total initial state area ( $A_1 + A_2$ ), as presented in formula (7). Figure 9 illustrates the schematic diagram for calculating the disintegration ratio corresponding to one dry-wet cycle.

$$D_R = \frac{A_1}{A_1 + A_2} \quad (7)$$

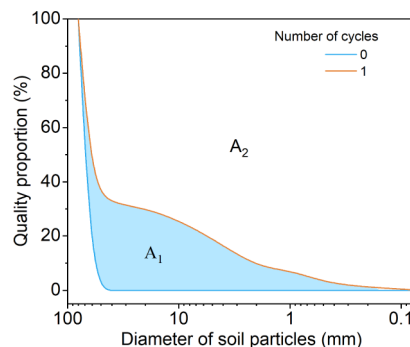


Figure 9. Schematic diagram for calculating  $D_R$ .

According to the definition of granularity entropy, values  $A$  and  $B$  were calculated after different dry-wet cycles, as shown in Table 3. Pearson correlation analysis was conducted on the number of dry-wet cycles, as well as variables  $A$ ,  $B$ , and  $D_R$ , as shown in Table 4. The correlation between  $A$  and  $D_R$  with the number of dry-wet cycles is significant, with  $p$ -values of 0.002 and 0.030, respectively. There is a significant negative correlation between  $A$  and  $D_R$ . Furthermore, while there is no significant correlation between  $B$  and the number of dry-wet cycles, a significant correlation with  $D_R$  is observed, with a  $p$ -value of 0.006.

A linear regression relationship between  $A$  and  $D_R$  was established, as illustrated in Figure 10. The results indicate that the disintegration ratio decreases as the standard basic entropy increases. This relationship is expressed in formula (8), which demonstrates a fitting degree of 0.984 and a significant linear negative correlation. There exists an inherent connection between  $A$  and  $D_R$ , with their physical meanings being relatively clear. These values reflect the degree of particle disintegration and fragmentation. Therefore, it is reasonable and feasible to use standard basic entropy as an indicator to describe the disintegration characteristics of expansive rocks. Specifically, a smaller value of  $A$  and a larger value of  $D_R$  correspond to a greater degree of particle disintegration and

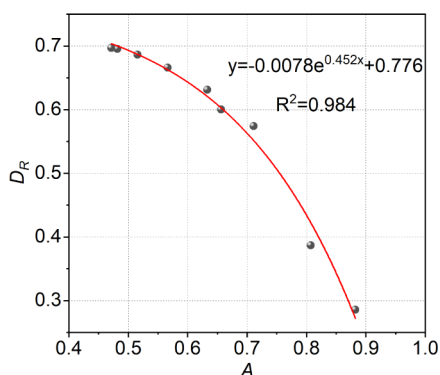
Table 3. Results of A and D<sub>R</sub> Calculations

Times	Particle content (%)											A	B	D <sub>R</sub>
	60~ 80	40~ 60	20~ 40	10~ 20	5~ 10	2~ 5	1~ 2	0.5~ 1	0.25~0.5	0.075~ 0.25	<0.075			
0	100	0	0	0	0	0	0	0	0	0	0	-	-	-
1	62.3	5.74	1.74	4.5	6.7	10.41	1.29	4.16	1.8	1.24	0.11	0.8822	0.84721	0.2854
2	47.52	0.96	5.86	5.29	4.9	20.27	1.8	9.12	2.2	1.91	0.17	0.8074	0.99412	0.3866
3	14.31	2.64	7.66	11.94	7.21	12.28	14.4	2.14	12.6	2.59	0.23	0.7111	1.24862	0.5740
4	7.61	4.28	10.26	9.13	12.51	26.21	3.38	14.94	6.71	4.4	0.56	0.6562	1.28771	0.6003
5	0	7.67	10.43	10.09	12.97	25.99	3.78	15.5	7.67	5.13	0.79	0.6330	1.25120	0.6313
10	0	2.26	6.6	10.15	12.3	27.13	4.68	18.84	9.48	7.33	1.24	0.5664	1.22497	0.6659
15	0	0	3.27	8.86	13.09	25.34	6.21	21.28	11.79	8.69	1.47	0.5157	1.18457	0.6864
20	0	0	1.25	6.69	12.59	25.07	6.24	22.35	13.9	10.27	1.64	0.4817	1.15931	0.6952
25	0	0	1.08	6.12	11.62	25.32	6.2	22.19	14.65	11.07	1.75	0.4715	1.15522	0.6970

Table 4. Pearson Correlation Analysis<sup>a</sup>

	Variable	Times	A	B	D <sub>R</sub>
Times	Pearson correlation	1			
	Significance				
A	Pearson correlation	-0.883**	1		
	Significance	0.002			
B	Pearson correlation	0.233	-0.628	1	
	Significance	0.547	0.070		
D <sub>R</sub>	Pearson correlation	0.716*	-0.954**	0.828**	1
	Significance	0.030	0.000	0.006	

<sup>a</sup>Note: \*\*. At the 0.01 level (double tailed), the correlation is significant. \*. At the 0.05 level (double tailed), the correlation is significant.

Figure 10. Relationship between standard basic entropy(A) and disintegration ratio (D<sub>R</sub>).

fragmentation. This finding is consistent with the research conducted by Zeng et al.<sup>35</sup>

$$y = -0.0078e^{0.452x} + 0.776 \quad (8)$$

The relationship between standard basic entropy and the number of dry-wet cycles is illustrated in Figure 11, with the fitted relationship represented by Formula (9). The goodness of fit is as high as 0.994, indicating a strong correlation between standard basic entropy and the number of dry-wet cycles. This finding is generally consistent with the research conducted by Zhang et al.<sup>36</sup> Initially, as the number of dry-wet cycles increases, the standard basic entropy rapidly decreases before gradually approaching a stable value. Coarse particles disintegrate quickly into fine particles, leading to a sharp increase in the fine particle content. However, the disintegration of fine particles diminishes over time. Once all coarse particles have disintegrated, the particle size distribution

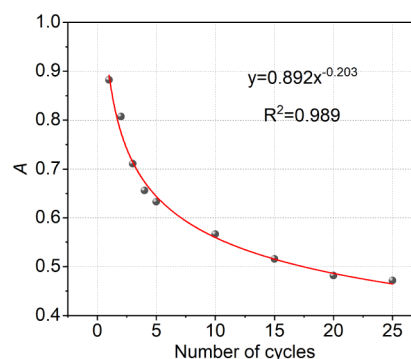


Figure 11. Change in standard basic entropy (A) with the number of cycles.

stabilizes. Therefore, standard basic entropy serves as a reliable indicator of the variation in particle characteristics during CBS disintegration in relation to the number of dry-wet cycles.

$$y = 0.892x^{-0.203} \quad (9)$$

**4.3. The Influence of WTF on Disintegration.** Figure 12 illustrates the calculation of bubble pressure. As depicted in

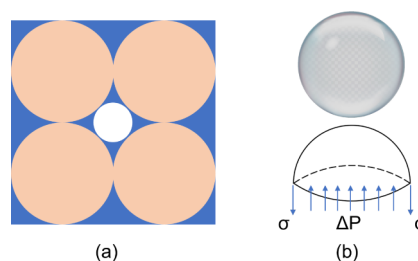
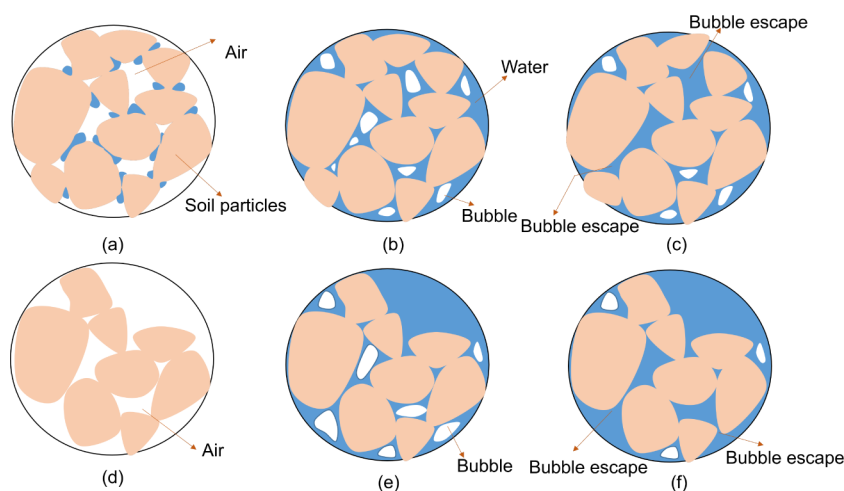


Figure 12. Calculation sketch of bubble pressure: (a) bubble formed by water-filling, (b) bubble force analysis diagram.

Figure 12a, when CBS is immersed in water, the water is continuously transported into the soil, gradually compressing the air bubbles and increasing their internal pressure. Eventually, a balance of forces is achieved, whereby the pressure of the bubbles equals the tension of the water. For mechanical analysis, the bubble is bisected as shown in Figure 12b, leading to eq 10, which can be simplified to obtain eq 11.<sup>37,38</sup> The surface tension coefficient of water varies with temperature; at 20 °C, it is approximately  $72.6 \pm 0.2$  mN/m. Based on the analysis in Figure 12a, it is assumed that the maximum diameter  $D_b$  of the bubbles is approximately equal to the average diameter of the pores, which is estimated to be



**Figure 13.** Influence of WTF on the disintegration process of CBS: (a) initial state of CBS, (b) CBS filled with water, (c) escape bubbles, (d) CBS drying, (e) CBS filled with water again, (f) escaping bubbles and CBS disintegration.

13.5  $\mu\text{m}$  according to the pore parameters calculated in Table 2. Consequently, the average air pressure within the bubble is estimated to be approximately 12.5 kPa. However, some pore diameters are significantly smaller than the average pore size, with values as low as 0.5  $\mu\text{m}$ , leading to a calculated air pressure of 580.8 kPa. This pressure can have a substantial destructive effect on CBS that are filled with cracks. These findings are generally consistent with the calculation methods reported in the literature.<sup>39</sup>

$$\frac{\pi}{4} D_b^2 \Delta P = \pi D_b \sigma \quad (10)$$

$$\Delta P = \frac{4\sigma}{D_b} \quad (11)$$

where  $\Delta P$  is the pressure of the bubble,  $\sigma$  is the surface tension coefficient of water, and  $D_b$  is the diameter of the bubble.

Figure 13 illustrates the influence of WTF on the disintegration process of CBS. Figure 14 presents physical

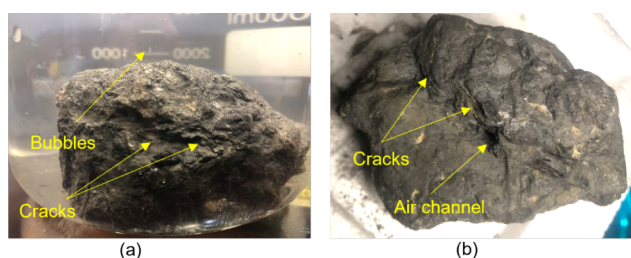


**Figure 14.** Physical images from the static water test of CBS: (a) physical image of CBS in immersion water, (b) Physical drawing of CBS after drying.

images from the static water test conducted on CBS. A Representative Elementary Volume (REV) was selected in Figure 13 to analyze the disintegration of CBS.<sup>34,40</sup> The movement of WTF significantly impacts the disintegration of CBS during immersion tests. The moisture content of natural CBS is only 2.24%, and while there is WTF present in the pores, its proportion is minimal (Figure 13a). Due to strong matric suction, water quickly occupies the surface pores, sealing off the air escape channels (Figures 13b, 14a). Subsequently, water gradually migrates toward the internal

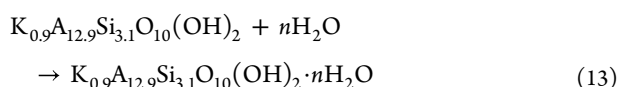
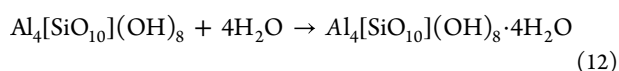
pores, compressing the air within them and causing the pressure to increase. When the air pressure reaches a critical level, it escapes at the nearest weak point. This escape of air can create channels from the interior to the exterior of the soft rock or directly damage the original soil structure (Figure 13c). After immersing the CBS samples in water, numerous bubbles can be observed escaping, and some weaker sections of the soil mass may collapse. Following the experimental procedure, the CBS is soaked for 12 h and then dried in an oven at 110 °C. After this process, water has mostly evaporated, and gas occupies all the pores (Figure 13d). The samples are then submerged in water for another 12 h, allowing water to reenter the pores and compress the gas inside them (Figure 13e). As the air pressure increases again, it continues to escape along weak areas, gradually forming through cracks or channels (Figure 13f; Figure 14b). During the dry-wet cycle experiments, WTF affects the structure of CBS in this manner. As the number of dry-wet cycles increases, cracks in CBS continue to propagate, eventually leading to disintegration. Overall, the physical images of the dry-wet cycles depicted in Figure 14 effectively validate the evolutionary process illustrated in Figure 13.

**4.4. The Influence of Mineral Composition on Disintegration.** According to Figure 1, the contents of kaolinite and Illite are 18.4% and 20%, respectively. The chemical formula of kaolinite is  $\text{Al}_4[\text{SiO}_{10}](\text{OH})_8$  or  $2\text{Al}_2\text{O}_3 \cdot \text{SiO}_2 \cdot 4\text{H}_2\text{O}$ .<sup>41,42</sup> Its chemical reaction with water is represented in formula (12). The crystal structure of kaolinite consists of a unit cell composed of a layer of aluminum oxide and a layer of silicon dioxide, which are bonded by chemical bonds. The strong interconnection between the unit cells makes it generally difficult for water molecules to penetrate, resulting in low hydrophilicity. While the crystal structure of kaolinite itself lacks expansibility, the surfaces of kaolinite clay particles contain free valence atoms and ions. These atoms and ions create an electrostatic attraction field on the surface of the clay particles. Water molecules, being dipoles with positive charges on one side and negative charges on the other, can be attracted to this electrostatic field. When clay particles come into contact with water, they form tightly arranged layers of water molecules, which thickens the bound water film around the clay particles and leads to macroscopic volume expansion. This



expansion is classified as a colloidal expansion mechanism within the physical and chemical expansion types.

The chemical formula of the Illite crystal is  $K_{0.9}A_{12.9}Si_{3.1}O_{10}(OH)_2$ . The crystal structure of Illite is similar to that of montmorillonite, with the distinction that Illite has a lower content of certain components in its three-layer crystal cell structure compared to montmorillonite.<sup>43,44</sup> Additionally, counterions are present between the unit cells of Illite. Upon contact with water, some of these counterions may escape, which reduces the attraction between the unit cells and allows water molecules to infiltrate. This infiltration results in an increase in the spacing between the unit cells, causing the mineral particles to expand, a phenomenon classified as molecular expansion. Previous studies have demonstrated that the physical and chemical interactions between Illite and water can lead to a 50% to 60% increase in the original volume of the rock. The chemical reaction process of water absorption and expansion in Illite is illustrated in formula (13).



The formation mechanism of water-hydrogen bonds is complex and not yet fully understood. Document<sup>45</sup> presents a semiempirical formula (14) for their hydration energy. Formula (15) is derived from the relationship between pressure and surface energy, as well as the Derjaguin approximation equation. This formula is then substituted into (14) to yield formula (16).

$$W_{HY} = A_1 e^{-\frac{D_L}{\lambda_1}} + A_2 e^{-\frac{D_L}{\lambda_2}} \quad (14)$$

$$P_{HY} = -\frac{dW_{HY}}{dD_L} = -\frac{d[(F/R)_{HY}/2\pi]}{dD_L} \quad (15)$$

$$P_{HY} = \frac{A_1}{\lambda_1} e^{-\frac{D_L}{\lambda_1}} + \frac{A_2}{\lambda_2} e^{-\frac{D_L}{\lambda_2}} \quad (16)$$

Among them,  $A_1, A_2$  is the energy level of primary and structural hydration;  $D_L$  is the interaction distance between clay mineral crystal layers;  $F$  is the interaction force between clay mineral crystal layers;  $R$  is the radius of curvature of the glass cylinder in the surface force tester; and  $W_{HY}$  is the total interaction energy between clay mineral crystal layers.

The unit layer thickness of the Illite crystal structure is 0.995 nm, while the interlayer domain measures 0.34 nm. eq 16 indicates that when the initial acting distance is 0.34 nm, the hydration repulsive pressure between the Illite crystal layers can reach 51.2–57.7 MPa. This pressure is sufficient to cause the crystal layers to expand and compromise the integrity of the crystal structure. However, the hydration force diminishes rapidly. Consequently, when the crystal layer spacing increases to approximately 1 nm, the hydration force decreases to only 1.5–3.6 MPa.<sup>46</sup> It can be confidently stated that the hydration of Illite is primarily attributed to short-range hydration repulsion. These changes are time-dependent; over time, mineral expansion tends to stabilize.

In summary, short-range hydraulic forces contribute to the formation of additional cracks in CBS. Granularity entropy is a critical parameter describing the uniformity of particle size

distribution within granular systems, significantly influencing the disintegration process of CBS. The physical and mechanical properties of CBS are notably affected by particle size, shape, and distribution. Conversely, the WTF is a primary factor influencing the stability and disintegration behavior of CBS. In such an environment, the particle size distribution of CBS directly impacts water permeability and air diffusivity. Seepage within unsaturated CBS involves WTF, where the air phase modifies water transport. Upon water immersion, hygroscopic pressure causes an increase in air pressure within the geotechnical matrix, leading to mineral skeleton disintegration along the weakest planes. It is important to note that high pore air pressure not only impedes water transport but also exacerbates the formation of cracks in the rock and soil mass. Most long-term studies on CBS slope failure concentrate on the strength attenuation characteristics of CBS. The water–air force coupling mechanism significantly influences the disintegration of CBS, thereby contributing to strength decay in CBS slopes. Understanding this mechanism is crucial for effective prevention and control of CBS slope instability.

## 5. CONCLUSIONS

This study performed static water decomposition, environmental scanning electron microscopy (ESEM), and mineral chemical composition analysis on intact CBS samples. The disintegration characteristics of CBS were evaluated using granularity entropy, and its disintegration mechanism was analyzed. The main conclusions are as follows:

- (1) The standard basic entropy ( $A$ ) effectively characterizes the particle properties of CBS during dry-wet cycles. A significant exponential relationship exists between  $A$  and the disintegration rate ( $D_R$ ), with  $D_R$  decreasing as  $A$  increases. This indicates that a smaller  $A$  corresponds to a higher degree of particle decomposition. As the number of dry-wet cycles increases, the standard basic entropy initially decreases rapidly before gradually approaching a constant value.
- (2) The variation of WTF is a critical factor influencing its decomposition. When water infiltrates, the pore channels close, resulting in the escape of pressurized air from the weaker areas of the structure. This continuous release of air leads to the formation of cracks or channels. Throughout the dry-wet cycles, WTF migrates persistently, ultimately contributing to soil disintegration.
- (3) The crystals of kaolinite and Illite chemically react with water to form new chemical compounds that exert an expansive effect on soil structure. Illite generates significant short-range hydration repulsion, leading to the formation of additional cracks in CBS. The migration of WTF exacerbates the degradation of CBS due to the formation of fractures, ultimately leading to structural collapse.


However, the impact of WTF on disintegration discussed in this article remains insufficiently explored, and the microscopic mechanisms and quantitative characterization of its effects will be the focus of future research.

## AUTHOR INFORMATION

### Corresponding Author

Mingxin Zheng — College of Transportation Engineering, East China Jiaotong University, Nanchang, Jiangxi 330013,



China;  [orcid.org/0000-0001-9792-4223](https://orcid.org/0000-0001-9792-4223);  
Email: [zhengmingxin0317@yeah.net](mailto:zhengmingxin0317@yeah.net)

## Authors

**Guanji Lyu** – College of Transportation Engineering, East China Jiaotong University, Nanchang, Jiangxi 330013, China; Department of Management Engineering, Fujian Business University, Fuzhou, Fujian 350012, China

**Lu Xiong** – College of Transportation Engineering, East China Jiaotong University, Nanchang, Jiangxi 330013, China

**Zilong Liu** – College of Transportation Engineering, East China Jiaotong University, Nanchang, Jiangxi 330013, China

**Hanqiu Zhang** – College of Transportation Engineering, East China Jiaotong University, Nanchang, Jiangxi 330013, China

Complete contact information is available at:

<https://pubs.acs.org/10.1021/acsomega.4c09569>

## Author Contributions

M.Z.: Conceptualization, writing, and reviewing the manuscript. G.L.: methodology, resources, drawing figures, and writing the manuscript. L.X. and Z.L.: data curation. H.Z.: investigation and validation.

## Notes

The authors declare no competing financial interest.

## ACKNOWLEDGMENTS

This research was supported by the National Natural Science Foundation of China (Grant Number 51568022), the Major Project of the Jiangxi Provincial Natural Science Foundation (Grant Number 20242BAB26078), and the Project of Fujian Business University (Grant Number SYHX202450).

## REFERENCES

- (1) Huang, G.; Zheng, M. Strength of Vegetated Coal-Bearing Soil under Dry-Wet Cycles: An Experimental Study. *Int. J. Corros.* **2021**, *2021*, 1–13.
- (2) Zhao, J.; Lu, C.; Deng, L.; Liu, G. Impacts of Simulated Acid Solution on the Disintegration and Cation Release of Purple Rock (Mudstone) in Southwest China. *Geomorphology* **2018**, *316*, 35–43.
- (3) Han, B.; Lu, G.; Zhu, Z.; Guo, Y.; Zhao, Y. Microstructure Features of Powdery Coal-Bearing Soil Based on the Digital Image Measurement Technology and Fractal Theory. *Geotech. Geol. Eng.* **2019**, *37*, 1357–1371.
- (4) Meng, Z.; Shi, X.; Li, G. Deformation, Failure and Permeability of Coal-Bearing Strata During Longwall Mining. *Eng. Geol.* **2016**, *208*, 69–80.
- (5) Mišćević, P.; Vlastelica, G. Estimation of Embankment Settlement Caused by Deterioration of Soft Rock Grains. *Bull. Eng. Geol. Environ.* **2019**, *78*, 1843–1853.
- (6) Zhang, H.; Liu, G.; Chen, W.; Guo, G.; Xia, Z.; Li, B.; Li, Z.; Cao, P. Failure Investigation of the Tunnel Lining in Expansive Mudstone – a Case Study. *Eng. Fail. Anal.* **2024**, *158*, 108003.
- (7) Chen, L.; Liu, T.; Jia, B.; Tang, J.; Liu, J. Acoustic Emission and Fractal Characteristics of Red Beds Soft Rock under Water-Force Coupling. *Sci. Rep.* **2024**, *14* (1), 4424.
- (8) Zhang, Z.; Gao, W. Effect of Different Test Methods on the Disintegration Behaviour of Soft Rock and the Evolution Model of Disintegration Breakage under Cyclic Wetting and Drying. *Eng. Geol.* **2020**, *279*, 105888.
- (9) Ding, L.; Liu, Y. Study on the Fractal Model of Erosion of Soft Rock by Water Immersed: Case Study Erosion of Metamorphic Slate. *Geotech. Geol. Eng.* **2021**, *39*, 5183–5189.
- (10) Doostmohammadi, R.; Moosavi, M.; Mutschler, T.; Osan, C. Influence of Cyclic Wetting and Drying on Swelling Behavior of Mudstone in South West of Iran. *Environ. Geol.* **2009**, *58* (5), 999–1009.
- (11) Gautam, T. P.; Shakoor, A. Slaking Behavior of Clay-Bearing Rocks During a One-Year Exposure to Natural Climatic Conditions. *Eng. Geol.* **2013**, *166*, 17–25.
- (12) Youn, H.; Tonon, F. Effect of Air-Drying Duration on the Engineering Properties of Four Clay-Bearing Rocks in Texas. *Eng. Geol.* **2010**, *115*, 58–67.
- (13) Zhang, Z.; Han, L.; Wei, S.; Chen, L.; Liu, G.; Zhang, L. Disintegration Law of Strongly Weathered Purple Mudstone on the Surface of the Drawdown Area under the Conditions of Three Gorges Reservoir Operation. *Eng. Geol.* **2020**, *270*, 105584.
- (14) Bonto, M.; Welch, M. J.; Lüthje, M.; Andersen, S. I.; Veshareh, M. J.; Amour, F.; Afrough, A.; Mokhtari, R.; Hajiabadi, M. R.; Alizadeh, M. R.; et al. Challenges and Enablers for Large-Scale CO<sub>2</sub> Storage in Chalk Formations. *Earth Sci. Rev.* **2021**, *222*, 103826.
- (15) Sumner, P. D.; Hall, K. J.; van Rooy, J. L.; Meiklejohn, K. I. Rock Weathering on the Eastern Mountains of Southern Africa: Review and Insights from Case Studies. *J. Afr. Earth Sci.* **2009**, *55*, 236–244.
- (16) Fan, Y.; Zheng, M.; Wu, J. A Study on the Shear Strength Characteristics and Microscopic Mechanism of Coal-Bearing Soil under Dry-Wet Cycles. *Front. Earth Sci.* **2023**, *10*, 1096980.
- (17) Fan, Y.; Zheng, M.; Wu, J. Experimental Research on Shear Strength Characteristics of Unsaturated Coal-Bearing Soils under Dry-Wet Circulation. *IOP Conf. Ser. Earth Environ. Sci.* **2021**, *719*, 042068.
- (18) Zhang, H.; Zheng, M.; Rong, Y.; Cui, M.; Cheng, K. Calibration and Sensitivity Analysis of Macro and Meso Parameters of Discrete Element Model for Coal Measure Soil. *J. Phys.: Conf. Ser.* **2023**, *2519* (1), 012036.
- (19) Huang, G.; Zheng, M. Effect of Dry-Wet Cycling on the Residual Strength Characteristics of Coal Measure Soil. *KSCE J. Civ. Eng.* **2021**, *25*, 4184–4195.
- (20) Gu, H.; Tao, M.; Li, X.; Li, Q.; Cao, W.; Wang, F. Dynamic Response and Failure Mechanism of Fractured Coal under Different Soaking Times. *Theor. Appl. Fract. Mech.* **2018**, *98*, 112–122.
- (21) Caron, J.; Espindola, C. R.; Angers, D. A. Soil Structural Stability During Rapid Wetting: Influence of Land Use on Some Aggregate Properties. *Soil Sci. Soc. Am. J.* **1996**, *60*, 901–908.
- (22) Zaher, H.; Caron, J. Aggregate Slaking During Rapid Wetting: Hydrophobicity and Pore Occlusion. *Can. J. Soil Sci.* **2008**, *88*, 85–97.
- (23) Grant, C. D.; Dexter, A. R. Generation of Microcracks in Molded Soils by Rapid Wetting. *Soil Res* **1989**, *27*, 169–182.
- (24) Zhang, B.; Feng, H.; Zhang, H. Influence of Particle Shape on Mechanical Properties of Coal Measure Soil by Discrete Element Method. *IOP Conf. Ser. Earth Environ. Sci.* **2020**, *455*, 012104.
- (25) Xie, G.; Hao, W. Identifying Organic Matter (Om) Types and Characterizing Om Pores in the Wufeng–Longmaxi Shales. *ACS Omega* **2022**, *7*, 38811–38824.
- (26) Ke, Q.; Li, C.; Yao, W.; Fan, Y.; Zhan, H.; Li, B.; Zhang, X. Comparative Characterization of Sandstone Microstructure Affected by Cyclic Wetting-Drying Process. *Int. J. Rock Mech. Min. Sci.* **2023**, *170*, 105486.
- (27) Tan, A.; Shi, S.; Wu, W.-Z.; Li, J.; Pedrycz, W. Granularity and Entropy of Intuitionistic Fuzzy Information and Their Applications. *IEEE Trans. Cybern.* **2020**, *52*, 192–204.
- (28) Asenjo, D.; Paillusson, F.; Frenkel, D. Numerical Calculation of Granular Entropy. *Phys. Rev. Lett.* **2014**, *112*, 098002.
- (29) Pachter, J. A.; Yang, Y.-J.; Dill, K. A. Entropy, Irreversibility and Inference at the Foundations of Statistical Physics. *Nat. Rev. Phys.* **2024**, *6*, 382–393.
- (30) Xia, X.; Qiang, Z.; Bass, G.; Becker, M. L.; Vogt, B. D. Morphological Control of Hydrothermally Synthesized Cobalt Oxide Particles Using Poly(Vinyl Pyrrolidone). *Colloid Polym. Sci.* **2019**, *297*, 59–67.
- (31) Li, X.; Chen, Q.; Liu, Z.; Zhou, C.; Wang, C.; Chen, C. A Refined Representation Method of the Particle Size Distribution Curve Based on Grading Entropy. *Particuology* **2024**, *88*, 302–311.

- (32) Cheshmberah, F.; Zolfaghari, A. A.; Taghizadeh-Mehrjardi, R.; Scholten, T. Evaluation of Mathematical Models for Predicting Particle Size Distribution Using Digital Soil Mapping in Semiarid Agricultural Lands. *Geocarto Int.* **2022**, *37*, 13016–13038.
- (33) Zhang, G.; Ling, S.; Wu, X. Evolution of Disintegration Breakage of Upper Cretaceous Red-Bed Mudstone in an Acidic Environment Based on the Weibull Model. *Acta Geotech.* **2023**, *18*, 6573–6593.
- (34) Erguler, Z. A.; Shakoor, A. Relative Contribution of Various Climatic Processes in Disintegration of Clay-Bearing Rocks. *Eng. Geol.* **2009**, *108*, 36–42.
- (35) Zeng, Z.; Kong, L.-W.; Tian, H.; Li, J.-Z. Effect of Drying and Wetting Cycles on Disintegration Behavior of Swelling Mudstone and Its Grading Entropy Characterization. *Rock And Soil Mechanics* **2017**, *38*, 1983–1989.
- (36) Zhang, Z.; Gao, W.; Tang, X.; Zhang, J.; Han, S. Characteristics of Grading Entropy of Disintegration of Swelling Rock under Dry-Wet Cycles. *J. Water Resour. Water Eng.* **2019**, *30*, 218–224.
- (37) Lee, S.; Kim, D. H.; Needham, D. Equilibrium and Dynamic Interfacial Tension Measurements at Microscopic Interfaces Using a Micropipet Technique. 1. A New Method for Determination of Interfacial Tension. *Langmuir* **2001**, *17*, 5537–5543.
- (38) Lee, S.; Kim, D. H.; Needham, D. Equilibrium and Dynamic Interfacial Tension Measurements at Microscopic Interfaces Using a Micropipet Technique. 2. Dynamics of Phospholipid Monolayer Formation and Equilibrium Tensions at the Water–Air Interface. *Langmuir* **2001**, *17*, 5544–5550.
- (39) Kinoshita, K.; Parra, E.; Needham, D. New Sensitive Micro-Measurements of Dynamic Surface Tension and Diffusion Coefficients: Validated and Tested for the Adsorption of 1-Octanol at a Microscopic Air-Water Interface and Its Dissolution into Water. *J. Colloid Interface Sci.* **2017**, *488*, 166–179.
- (40) Wu, M.; Wu, J.; Wu, J.; Hu, B. X. A Three-Dimensional Model for Quantification of the Representative Elementary Volume of Tortuosity in Granular Porous Media. *J. Hydrol* **2018**, *557*, 128–136.
- (41) Bentabol, M.; Abad, I. Solid Solutions in Micas Hydrothermally Synthesized from Kaolinite at 400 °C. *Appl. Clay Sci.* **2019**, *182*, 105279.
- (42) Li, Y.; Liu, Q.; Liu, L.; Liu, L.; Hou, D.; Wu, Y. Effect of Original Crystal Size of Kaolinite on the Formation of Intercalation Compounds of Coal-Measure Kaolinite. *Mater. Today Commun.* **2023**, *35*, 106130.
- (43) Clauer, N.; Williams, L. B.; Lemarchand, D.; Florian, P.; Honty, M. Illitization Decrypted by B and Li Isotope Geochemistry of Nanometer-Sized Illite Crystals from Bentonite Beds, East Slovak Basin. *Chem. Geol.* **2018**, *477*, 177–194.
- (44) Blaise, T.; Clauer, N.; Cathelineau, M.; Boiron, M.-C.; Techer, I.; Boulvais, P. Reconstructing Fluid-Flow Events in Lower-Triassic Sandstones of the Eastern Paris Basin by Elemental Tracing and Isotopic Dating of Nanometric Illite Crystals. *Geochim. Cosmochim. Acta* **2016**, *176*, 157–184.
- (45) Kilpatrick, J. I.; Loh, S.-H.; Jarvis, S. P. Directly Probing the Effects of Ions on Hydration Forces at Interfaces. *J. Am. Chem. Soc.* **2013**, *135*, 2628–2634.
- (46) Kang, Y.; Yang, B.; Li, X.; Yang, J.; You, L.; Chen, Q. Quantitative Characterization of Micro Forces in Shale Hydration and Field Applications. *Pet. Explor. Dev.* **2017**, *44* (2), 328–335.